Journal of Inorganic Biochemistry 260 (2024) 112702

Contents lists available at ScienceDirect

Journal of Inorganic Biochemistry

journal homepage: www.elsevier.com/locate/jinorgbio

Bridging pyrimidine hemicurcumin and Cisplatin: Synthesis, coordination chemistry, and *in vitro* activity assessment of a novel Pt(II) complex

Matteo Mari [a], Matteo Boniburini [a], Marianna Tosato [a,b], Francesca Zanni [a], Filippo Bonini [a], Francesco Faglioni [a], Laura Cuoghi [c], Silvia Belluti [c], Carol Imbriano [c], Mattia Asti [b], Erika Ferrari [a,*]

[a] Department of Chemical and Geological Sciences, University of Modena and Reggio Emilia, via Campi, 103, 41125 Modena, Italy
[b] Radiopharmaceutical Chemistry Section, Nuclear Medicine Unit, Azienda USL-IRCCS Reggio Emilia, via Amendola 2, 42122 Reggio Emilia, Italy
[c] Department of Life Sciences, University of Modena and Reggio Emilia, via Campi, 213/d, 41125 Modena, Italy

ARTICLE INFO

Keywords:
Platinum-based drugs
Oxaliplatin
Curcumin derivatives
Nuclear Magnetic Resonance
Density Functional theory
Amino-pyrimidine

ABSTRACT

In the upcoming decades, the incidence and mortality rates of cancer are expected to rise globally, with colorectal and prostate cancers among the most prevalent types. Despite advancements in molecular targeted therapy, platinum-based chemotherapies remain the cornerstone of treatment, especially for colorectal and prostate cancer, with oxaliplatin and cisplatin being extremely effective due to their DNA-targeting capabilities. In our pursuit of new platinum-based chemotherapeutics that are potentially less toxic and more effective, we have explored the combination of the Pt-binding groups of the diaminocyclohexane ring used in oxaliplatin, with the stable amino-pyrimidine hemicurcumin moiety. This new derivative exhibit improved stability in physiological conditions and increased solubility in aqueous media, demonstrating promising effects on cell proliferation of both colorectal and prostate cells. We report herein the complete synthesis and chemical characterization in solution of the new derivative [(1*R*,2*R*)-N1-(3-(4-((*E*)-2-(2-Amino-6-methylpyrimidin-4-yl)vinyl)-2-methoxyphenoxy) propyl) cyclohexane-1,2-diamine] (MPYD). Our analysis includes an examination of its acid-base equilibria, speciation and stability in physiological conditions. The synthesis and *in situ* formation of Pt(II) complexes were investigated by nuclear magnetic resonance spectroscopy, while density functional theory calculations were employed to elucidate the chemical structure in solution. Results on the biological activity were obtained through cell viability assays on different colorectal and prostate cell lines (HCT116, HT29, PC3 and LNCaP).

1. Introduction

According to the World Cancer Research Fund International, colorectal (CRC) and prostate (PCA) cancers are among the most commonly occurring cancers worldwide. CRC is the third most common cancer in both men and women, while PCA is the second most common in men, respectively [1]. This ranking underscores the significant impact these tumors have on health globally. Although screening-based early detection and treatments for both cancers have improved over the last few decades, reducing the mortality rate compared to other cancers, CRC and PCA are still significant causes of cancer-related deaths worldwide.

Despite recent developments in molecular targeted therapy, chemotherapy still remains the bedrock of CRC treatment, both in first-line single-agent therapy and in combined regimens such as, for instance, the FOLFOX that associates folinic acid, 5-fluorouracil (5-FU), and oxaliplatin (OX), a well-known and widely used third-generation platinum-based pharmaceutical, mostly targeting DNA and blocking its replication [2]. Although chemotherapy based on taxanes represents one of the clinically approved most effective treatments for prostate cancers [3], the development of taxane resistance remains a major challenge especially for castration resistant prostate cancer [4]. Recently, platinum-based compounds, whose progenitor is Cisplatin (*cis*-diamminedichloroplatinum(II) - CDDP) are under investigations in several clinical trials for defeating castration-resistant and hormone-sensitive PCA [5–7].

Typical features of platinum-based chemotherapeutics such as OX

* Corresponding author.
E-mail addresses: lacuoghi@unimore.it (L. Cuoghi), silvia.belluti@unimore.it (S. Belluti), carol.imbriano@unimore.it (C. Imbriano), mattia.asti@ausl.re.it (M. Asti), erika.ferrari@unimore.it (E. Ferrari).

https://doi.org/10.1016/j.jinorgbio.2024.112702
Received 28 June 2024; Received in revised form 5 August 2024; Accepted 15 August 2024
Available online 20 August 2024

and CDDP are the presence of two *cis*-labile groups and two strongly bound *cis N*-ligands. Intracellularly, labile ligands are exchanged with water molecules to form the aquo-platinum complex that, in turn, enters into the nucleus to form DNA adducts by coordination of the *cis*-[Pt(R-NH_2)$_2$] fragment [8–10]. The formation of cross-link adducts, typically with guanosine and adenosine residues, lead to an impairment of DNA expression. Recently, Bruno et al. [11] demonstrated that, despite the similar chemical structure of the metal center, the ability of oxaliplatin to cross-link DNA might be of little significance in its cytotoxicity, since the DNA-damage response is not activated. Indeed, oxaliplatin-modified DNA could still lead to the inhibition of rRNA synthesis, which would ultimately be responsible for ribosome biogenesis stress. Concerning the coordination sphere of platinum in OX, the *cis*-N ligands are provided by the chelating site diaminocyclohexane (DACH) that, combining bulkiness and positive inductive effects, allows to slow down substitution reactions in the square planar coordination sphere of Pt(II), thus reducing the rate of the aquation reaction. This improved inertness possibly diminishes its physiological side-effects [12,13], especially those due to the binding to sulfur-donor endogen molecules such as proteins, enzymes and glutathione. The presence of additional substituents on the *N*-ligands may also account for hampering the cellular repairing mechanism and enhancing therapeutic activity. Moreover, if the bulky substituents have to some extent therapeutic activities, the final compound could benefit from these as well.

In this scenario, searching for new, possibly less toxic, and more active Pt-based chemotherapeutics, we have functionalized the stable amino-pyrimidine hemicurcumin moiety with the DACH Pt-chelating group. Curcumin has shown a wide range of exciting potential therapeutic features *in vitro* [14–19], sadly disappointed by the outcomes of the *in vivo* applications. The poor therapeutic success of curcumin is mostly due to a combination of detrimental features, such as its high instability in physiological conditions as well as its poor uptake and bioavailability [20–22]. In the last decades, many efforts have been carried out to overcome these issues, particularly in designing and synthesizing improved analogues. Among them, aminopyrimidine-curcumin derivatives have been recently investigated and showed improved stability in physiological conditions and higher solubility in aqueous media. Additionally, the effects of these molecules on cell proliferation of both CRC and PCA cells were tested [23]. Although the antiproliferative activity of aminopyrimidine hemicurcumin derivatives was found weaker if compared to the lead compound [23] and only androgen-sensitive PCA cells (LNCaP) are effectively inhibited, aminopyrimidine-hemicurcumin moiety can be used as a pivotal molecule to develop new Pt-based drugs potentially targeting PCA and CRC cancer. The new Pt(II) complex could take advantage of the aminopyrimidine-hemicurcumin moiety as well as the metallic core.

The whole synthesis of the new DACH-derivative [(1*R*,2*R*)-N1-(3-(4-((*E*)-2-(2-amino-6-methylpyrimidin-4-yl)vinyl)-2-methoxyphenoxy) propyl) cyclohexane-1,2-diamine] (**MPYD, L, 5**) is reported herein together with its full chemical characterization in solution, comprising the acid-base equilibria, speciation and stability in physiological conditions. The synthesis and *in situ* formation of Pt(II) complexes, investigated by nuclear magnetic resonance (NMR) spectroscopy and density functional theory (DFT) calculations, allowed unravelling the chemical structure in solution. Preliminary results on the biological activity were collected by cell viability assays on different CRC and PCA cell lines (HCT116, HT29, PC3 and LNCaP).

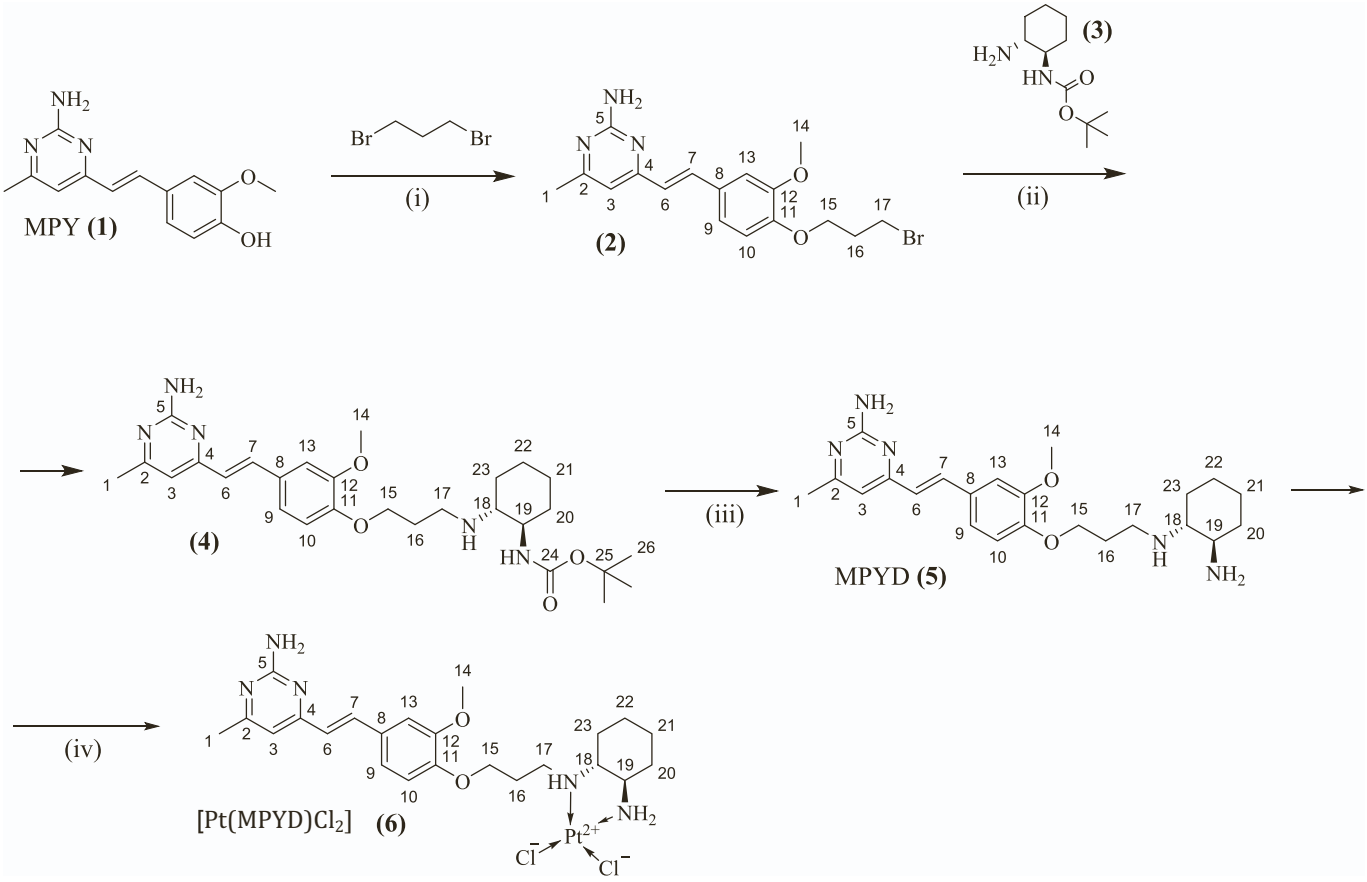

Fig. 1. Full reaction scheme for the synthesis of MPYD (**5**) and [Pt(MPYD)Cl_2] (**6**). i) DMF, Cs_2CO_3, RT, 48 h; (ii) DMF, Cs_2CO_3, RT, 24 h; (iii) DCM, TFA, RT, 90 min; (iv) H_2O, K_2PtCl_4, RT, 24 h.

2. Results

2.1. Synthesis

The full reaction scheme for the synthesis of MPYD (**5**) and its Pt(II) chloro-complex is reported in Fig. 1. 4-(2-(2-Amino-6-methylpyrimidin-4-yl)vinyl)-2-methoxyphenol (MPY, **1**) was synthesized through an aldol-like condensation between vanillin and 2-amino-4,6-dimethyl pyrimidine, as previously reported [23]. MPY reacts *via* nucleophilic substitution (S_N2) with 1,3-dibromopropane in DMF in the presence of Cs_2CO_3 to form the bromopropyl-derivative (**2**) in good yield (65%), being the combination of dry DMF and cesium carbonate extremely favourable for alkylating phenolic oxygen [24]. The polar anhydrous solvent promotes the formation of a "naked" anion (phenoxide), which acts as a strong nucleophile and allows the reaction to be carried out at room temperature achieving good yield. The insertion of DACH in the structure of **2** was performed in similar conditions, indeed Cs_2CO_3 mainly promotes the alkylation of primary amines rather than secondary ones, hence avoiding the formation of tertiary amines [25,26]. The asymmetric synthesis requires the Boc-protection of one amine group as previously reported for similar compounds [27]. After Boc-deprotection of **4** by TFA, MPYD (**5**) was isolated.

In solution, only the *E* isomer of MPYD is observed as shown by the ^{1}H NMR spectrum (Fig. S1) in which the two doublets at 6.90 and 7.62 ppm corresponding to the vinylic protons H-6 and H-7 have a coupling constant $^3J_{HH}$ equal to 16.0 Hz, typical of alkene protons in the *trans* configuration. The aliphatic region of the spectrum is quite complicated due to the presence of an asymmetrically substituted cyclohexane ring, in which all the protons are not chemical shift equivalent. Also, propyl methylene protons (H-17) bound to nitrogen are not chemical shift equivalent due to the presence of a pro-chiral nitrogen atom and the high-energy rotational barrier owing to the steric hindrance of bulky substituents.

The Pt(II) complex [Pt(MPYD)Cl_2] (**6**) was prepared following a direct complexation between MPYD (**5**) and K_2PtCl_4 in a 1:1 M ratio in ethanol/water (1:1 *V/V*) solution. This type of complexation in hydro-alcoholic media is well-documented in the literature, particularly for organic diamino-ligands with low water solubility [28–31]. The isolated yellow solid displayed poor solubility in water, methanol and nonpolar organic solvents, while it was soluble in DMSO and DMF.

2.2. Acid-base equilibria of MPYD

MPYD undergoes acid-base equilibria that play a key role in speciation in physiological conditions and for identifying favourable conditions for metal complexation. MPYD is characterized by five nitrogen-containing groups. Among them the pyrimidine ones are extremely acidic and totally deprotonated at pH > 2 [23]. Therefore, these pyrimidine groups were excluded from this investigation.

The overall protonation constants (β_{qr}) are defined by the following equations:

$$qL + rH^+ \rightleftharpoons [L_qH_r]^{(+r)} \quad (1)$$

$$\beta_{qr} = \frac{[L_qH_r^{+r}]}{[L]^q \bullet [H^+]^r} \quad (2)$$

where L is the ligand in the completely dissociated form and H is proton.

The protonation equilibria (Fig. 2) were determined using UV–Vis spectrophotometric data. As shown in Fig. 3, in acidic conditions (pH 2), MPYD exhibits an absorption peak with a maximum at $\lambda = 380$ nm. The absence of the phenolic group induces a hypsochromic shift, with a decrease in the wavelength of the maximum of absorbance of 20 nm in comparison to the lead compound MPY (λ_{max} 400 nm, [23]). As the pH increases, a blueshift is observed, with the maximum absorption shifting to 350 nm, accompanied by a decrease in absorbance (*i.e.* molar extinction coefficient). The overall protonation constants and pK_a values calculated from spectrophometric data using Hypspec [32] are summarized in Table 1.

The pK_{a1} value aligns with those obtained for similar amino pyrimidine groups [23]. However, the two amine groups bound to the cyclohexane ring in MPYD are slightly more acidic than those in DACH (5.79 *vs.* 6.21 and 8.83 *vs.* 9.60 for MPYD and DACH [33] respectively). For brevity, the neutral form of MPYD will be referred to as L in the following discussion. Under physiological conditions, the prevailing species is HL^+ (Fig. 4), in which the secondary ammine is protonated and the primary one is dissociated.

2.3. Complexation of Pt(II)

The complexing ability of MPYD towards Pt(II) was investigated in solution by NMR analysis. Although MPYD is highly soluble in methanol, DMSO and DMF, the NMR analysis in deuterated methanol (MeOD-d_4) was not feasible due to the precipitation of Pt(II) complex, thus excluding this solvent from the investigation. A 1:1 metal-to-ligand complex was formed by adding an aqueous $K_2[PtCl_4]$ solution to MPYD in DMSO. The complex formation proceeds slowly at room temperature, taking a few days to complete, as shown in Fig. 5. The complex and the free ligand are in fast exchange with respect to the NMR time scale, resulting in the shifts of the signals near the metallic core appearing as a weighted average of the free ligand's signals and those of

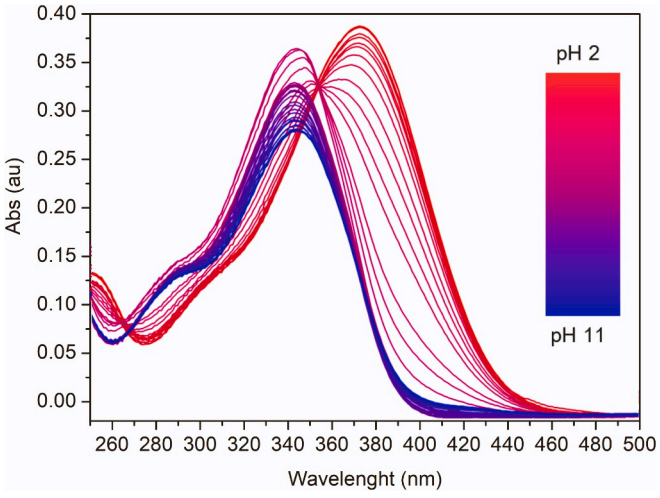

Fig. 3. UV–Vis pH-metric spectrophotometric titration of MPYD in aqueous solution (20 μM $MPYD_{tot}$; 0.1 M $NaNO_3$, 25 °C).

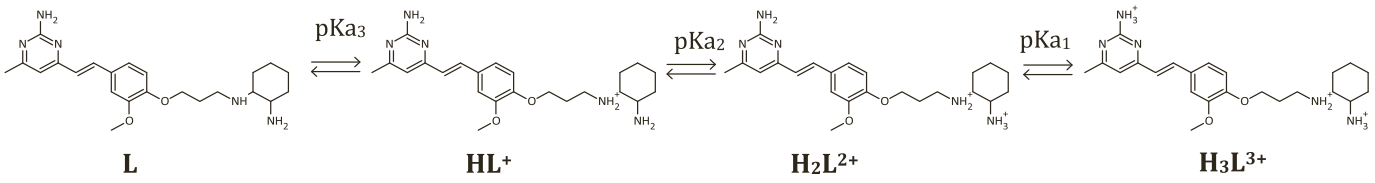

Fig. 2. Step protonation equilibria of MPYD.

Table 1
Overall protonation constants and pK_a values calculated from UV–Vis spectrophotometric data (0.1 M $NaNO_3$, 25 °C).

$\log\beta_{11}$	8.83 (3)
$\log\beta_{12}$	14.16 (3)
$\log\beta_{13}$	19.59 (3)
$pK_{a1} = \log\beta_{13} - \log\beta_{12}$	4.97 (9)
$pK_{a2} = \log\beta_{12} - \log\beta_{11}$	5.79 (6)
$pK_{a3} = \log\beta_{11}$	8.83 (3)

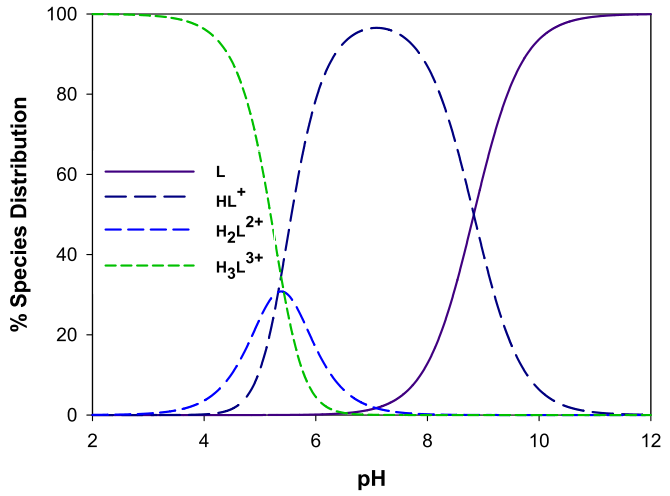

Fig. 4. Species distribution curves for MPYD calculated from overall protonation constants using PyES [34] (10^{-4} M L_{tot}; 0.1 M $NaNO_3$, 25 °C).

the Pt(II)-bound ligand. The aromatic protons remained unaffected by the metal additions, whereas the signals experiencing the greater downfield shifts are those in α position to coordinating amines, *i.e.* H-17, H-18 and H-19. Table 2 and Fig. S2 report the details of ^{1}H and ^{13}C chemical shifts and assignments for the free ligand and the Pt(II) complex. Consistently with previously reported Pt(II) complexes with substituted ethylenediamine (*en*) [35], the larger proton shifts are observed for methylene/methine groups attached to the secondary amine (C-17 and C-18). These proton signals exhibit line-broadening due to $^{3}J_{H\text{-}Pt}$ scalar coupling (~30–50 Hz). In addition, the formation of the metal complex restricts the free rotation of the propyl chain, inducing the splitting of H-15 and H-16 protons as a consequence of the non-chemical equivalency.

In addition to DMSO, the Pt(II) complex formation was investigated in DMF, a solvent with weaker coordinating properties than DMSO. Similarly, the investigation in DMF-d_7 pointed out the slow formation of the Pt(II) complex (Fig. S3). The chemical shift variation induced by the addition of the metal are quite similar in both solvents (Table 2, Table S1), although larger shifts are observed for H-17/17′ and H-18 in the presence of DMSO (Fig. S4).

The ^{1}H and ^{13}C NMR spectra obtained from the *in situ* addition of Pt(II) were compared with those of the isolated metal complex dissolved in DMF and DMSO. In each solvent, the resulting spectra are almost superimposable with slight shifts probably due to the different proton activity (a_{H^+}) induced by the direct addition of the metal to the solution. This is suggested by the downfield shift of H_2O/HDO residual signal observed when K_2PtCl_4 is added (see Fig. 5 last two spectra from the bottom).

2.4. DFT calculations

The ^{1}H and ^{13}C NMR chemical shifts were computed at the DFT level for the atoms close to the chelating amines for both the solvated MPYD molecule and two possible Pt(II) complexes.

Pt(II) coordination is assumed to occur with the chelating amine moieties of DACH (as observed by NMR) occupying two *cis* positions in the metal coordination sphere. The two remaining occupancies of the square planar geometry can be taken by either Cl^- ions or DMSO molecules. Based on both computed reaction energies and experimental clues, we considered two candidate stoichiometries for the Pt(II) complexes, namely $[PtLCl(DMSO)]^+$ and $[PtL(DMSO)_2]^{2+}$, and we mimicked these replacing MPYD with the smaller ligand (L^C) obtained by removing the pyrimidine-hemicurcumin fragment from L (Fig. S5), as the latter is not interacting with the metal centre. For each complex stoichiometry, as well as for L^C molecule in solution, several plausible geometric conformations were investigated. The resulting spectra are displayed in Fig. S6. Spin coupling constants were not included in the computation, so the simulated spectra do not contain multiplets due to signal splitting. The numerical values for the computed chemical shifts are reported in Tables S2 and S3.

2.5. Pharmacokinetic study in simulated physiological media

The stability of both ligand and its platinum complex were tested in simulated human plasma. The stability was investigated by means of UV–Vis spectroscopy inquiring spectral changes as function of time. As reported in Fig. S7, the ligand and the metal complex are extremely stable in the investigated physiological conditions; indeed, no significant spectral changes are observed. However, since the formation of the metal complex does not affect much the appearance of the absorption spectrum of the ligand, additional LC-MS experiments have been carried out to check the stability of the metal complex after 48 h in PBS buffer (37 °C, pH 7.4). The metal complex resulted extremely stable, showing the typical isotopic spectral pattern of platinum (Fig. S8) characterized by a parent peak at 678.2 *m/z* corresponding to the species $[PtLCl_2]$.

2.6. Inhibitory effects on the proliferation of human CRC and PCA cells

First, we evaluated the biological activity of MPYD (L) using cell viability assays in both colon (HCT116 and HT29) and prostate (LNCaP and PC3) cancer cell lines. The cells were treated with different concentrations of MPYD dissolved in DMSO for 48 h and cell viability was determined (Fig. 6). We previously characterized the lead compound MPY3 [4-{(*E*)-2-[4-(3-aminopropoxy)-3-methoxyphenyl]ethenyl}-6-methylpyrimidin-2-amine] (Fig. S9), which halved the percentage of LNCaP and HCT116 viable cells at 68.8 ± 21.7 μM and 98.0 ± 13.6 μM doses (IC_{50}), respectively, and was not active in HT29 and PC3 cells [23]. Conversely, MPYD was effective in all the tested cell lines, with the IC_{50} concentration being lower than MPY3 in both LNCaP and HCT116 cells (45.95 μM and 37.03 μM, respectively) (Table 3). The administration of MPYD to HCT116 cells for 72 h showed similar results (IC_{50} = 37.92 μM), indicating that the response to treatment occurs within 48 h (Fig. S10).

Next, we examined whether combining Pt(II) with MPYD would maintain, enhance, or decrease its biological effect on CRC and PCA cells. $[PtLCl_2]$ and MPYD (L) were dissolved in DMF to avoid the coordinating ability of DMSO on Pt(II) complexes [36] and dose-response effects were measured by cell viability assays after 48 h of treatment, as reported in Fig. 7. The comparison between cell viability curves (Fig. 7) and IC_{50} values (Table 4) highlighted a general decrease in the activity of $[PtLCl_2]$ compared to L. In particular, the Pt(II) complex lost its inhibitory effect on PCA cell viability (LNCaP and PC3), while increasing IC_{50} doses from 54.92 μM to 69.58 μM in HT29 and from 31.70 μM to 52.16 μM in HCT116 cancer cells.

Dose-response analysis in HCT116 cells at 72 h confirmed a lower activity of $[PtLCl_2]$ *versus* L. Nevertheless, $[PtLCl_2]$ showed a greater effect after 72 h (IC_{50} = 46.64 μM) compared to 48 h, that was not observed with MPYD (L), either dissolved in DMF (IC_{50} = 30.89 μM) or

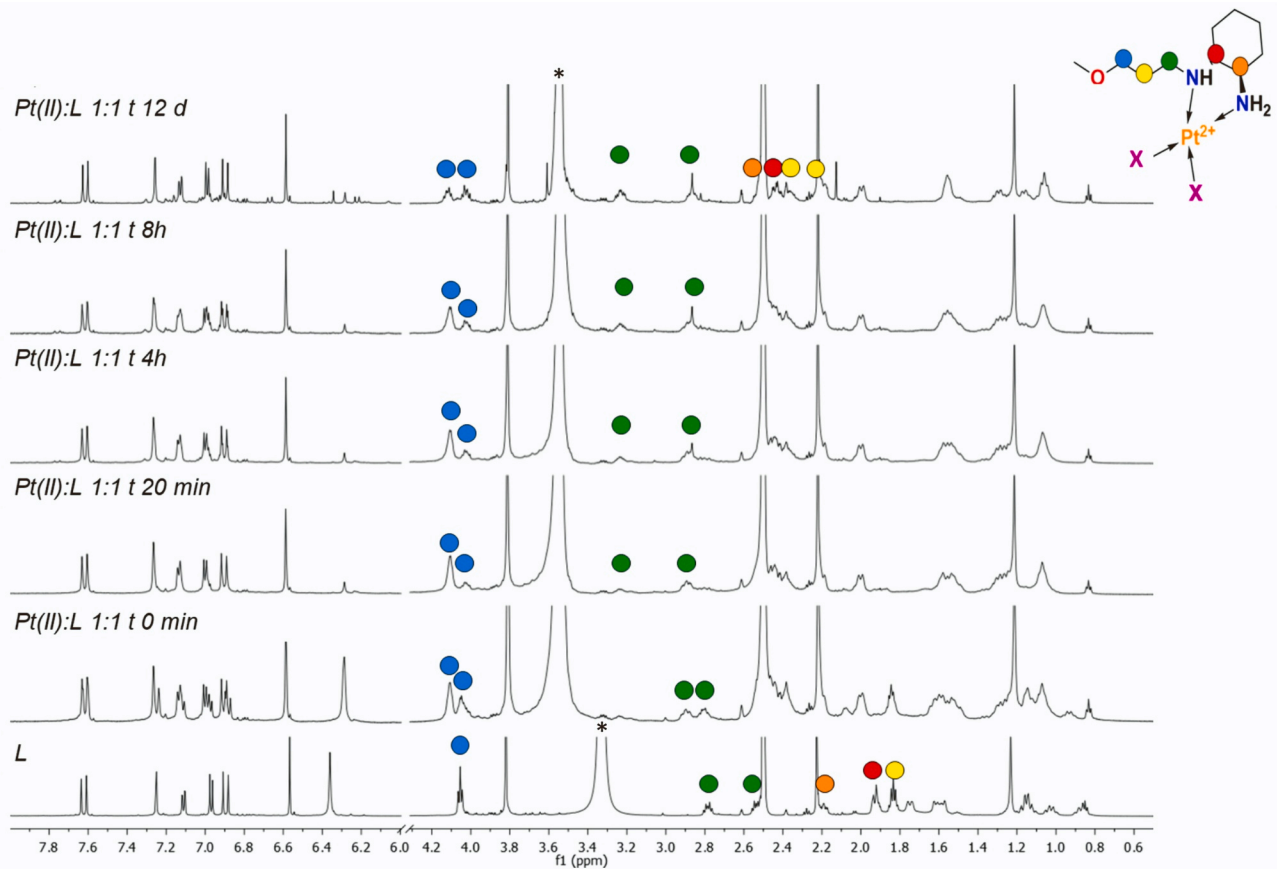

Fig. 5. ^{1}H NMR spectra of L and Pt(II):L 1:1 after different times from the addition of the metal solution, from time zero (second spectrum from bottom) to 12 days (top spectrum) (DMSO-d_6, 600 MHz, 25 °C). * residual HOD/H_2O signal.

Table 2
^{1}H and ^{13}C chemical shifts of methine/methylene groups in α position to the coordinating amines: free ligand (L) and the metal-to-ligand 1:1 system in DMSO-d_6 (600 MHz, 25 °C). Atom numbering refers to Fig. 1.

	δ (ppm)	15	16	17	18	19	20	21/22	23
L	^{1}H	4.063	1.842	2.547 2.794	1.929	2.196	1.758 1.040	1.61 1.159	1.942 0.881
	^{13}C	65.27	30.31	43.63	64.06	55.21	35.76	25.38	31.30
Pt:L 1:1	^{1}H	4.117 4.027	2.368 2.217	3.320 2.867	2.527	2.430	1.997 1.293	1.556 1.060	2.193 1.161
	^{13}C	66.26	27.36	43.01	64.61	60.63	32.15	24.43	28.13
Δδ (ppm)	^{1}H	+0.005 −0.040	+0.530 +0.380	+0.773 +0.070	+0.598	+0.234	+0.239 +0.253	−0.050 −0.100	+0.251 +0.280
	^{13}C	+0.990	−2.950	−0.62	0.55	+5.42	−3.61	−0.95	−3.18

in DMSO (Fig. S10). Oxaliplatin (OX) was administered as positive control for the efficacy of Pt(II)-based anti-cancer drugs in both CRC and PCA cells (Fig. S11).

To further investigate the biological activity of [$PtLCl_2$] compared to its ligand MPYD (L), we analysed cell cycle distribution of the cells treated with the molecules at IC_{50} doses for 48 h. As shown in Fig. 8, MPYD (L) exerted a robust apoptotic effect, with the SubG1 population increasing from 5.3% of DMF-treated cells to 47.3%, at the expense of G0/G1 cells that dropped from 66.3% to 29.7%. Differently, the administration of [$PtLCl_2$] mainly affected the replication phase, by reducing the S-phase population from 14.8% to 6.6%, and only slightly increased SubG1 events (from 5.3% to 12.5%). Oxaliplatin administration to HCT116 cells reduced S population (from 22.8% to 3.7%) and induced a G2/M cell cycle arrest (from 16.4% to 29.7%), consistently with literature data [37].

2.7. Cellular uptake

To check whether the reduced activity of [$PtLCl_2$] compared to OX could be ascribable to a lower uptake into cancer cells, we estimated the internalized Pt by inductively coupled plasma mass spectrometry (ICP-MS) in HCT116 cells previously treated for 6 h with [$PtLCl_2$] and OX at different doses (5, 20 and 50 μM). As shown in Fig. 9 (A), for the same dose of the two platinum complexes, different amounts of platinum were internalized in HCT116 cells, and higher values were detected for [$PtLCl_2$]. A dose/response trend is observed particularly for [$PtLCl_2$], suggesting a passive diffusion-driven uptake. If the incubation time is risen up to 48 h (Fig. 9, B), an increase in the platinum uptake (ng/10^6 cells) is observed for both compounds when tested at about their IC_{50} doses: OX (5 μM) 5.86 ± 0.34 ng (6 h) *vs.* 59.5 ± 36.7 ng (48 h); [$PtLCl_2$] (50 μM) 391.4 ± 27.1 ng (6 h) *vs.* 1070 ± 207 ng (48 h). Overall data are presented in Table 5.

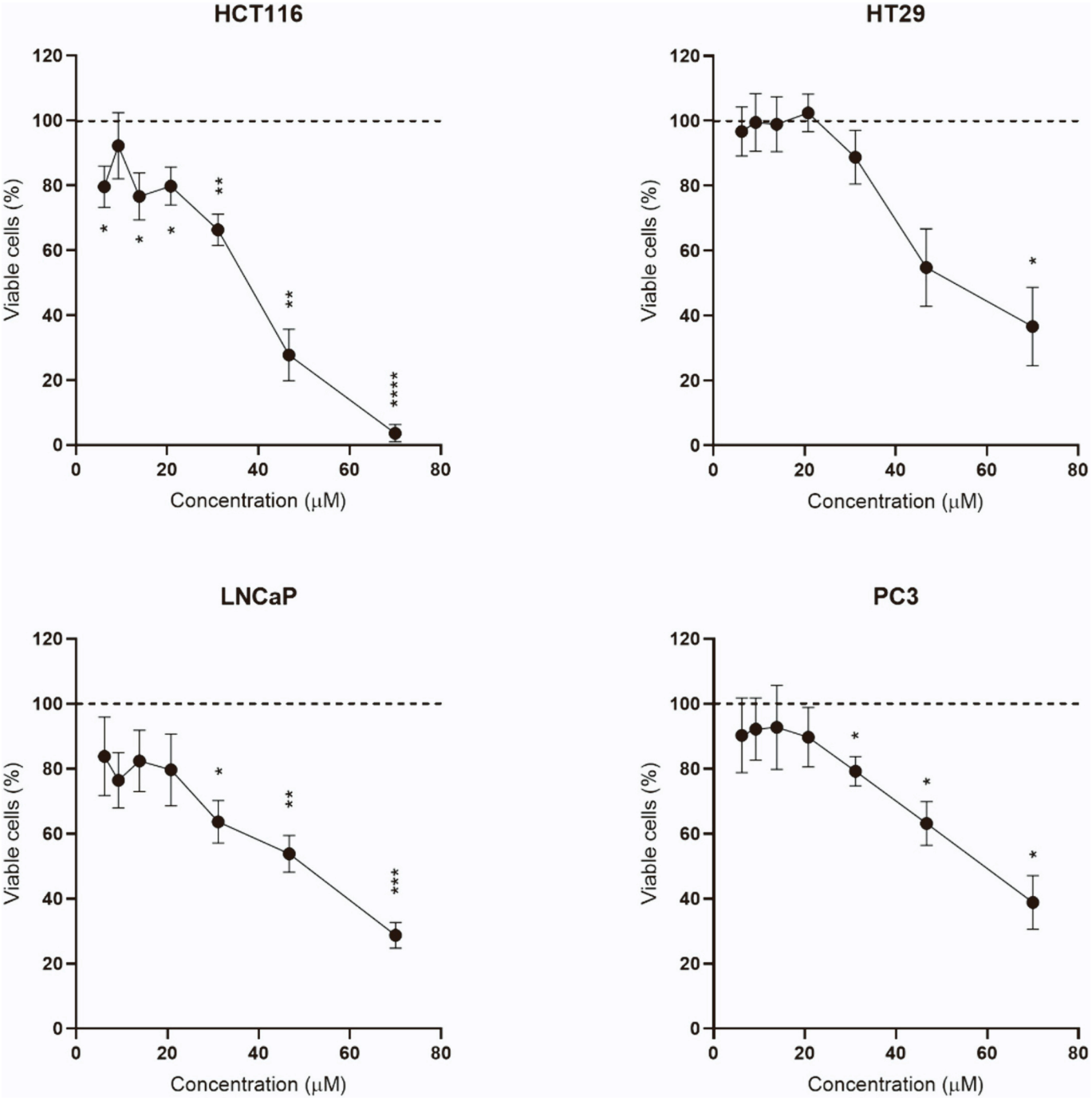

Fig. 6. Dose-dependent effect of MPYD on colon (HT29 and HCT116) and prostate (LNCaP and PC3) cancer cell lines. Cell viability of HCT116, HT29, LNCaP and PC3 cells was assessed after 48 h treatment with the indicated concentrations of MPYD (L) dissolved in DMSO. Data are presented as percentage of viable cells (%) following MYPD administration *versus* DMSO control cells, arbitrarily set at 100% (dashed line). Significance levels compared to DMSO treated cells (100%) are reported as $p < 0.05$ (*), $p < 0.01$ (**), $p < 0.001$(***).

Table 3
The drug concentration that reduces the cell population by 50% (IC_{50}) upon 48 h in the different cell lines is indicated as means ± SEM. Data were obtained from three independent experiments.

	IC_{50} (μM) ± SEM
HCT116	37.03 ± 2.72
HT29	60.63 ± 12.10
LNCaP	45.95 ± 3.53
PC3	60.62 ± 6.03

3. Discussion

MPYD is a new hemicurcumin derivative that combines a DACH moiety, acting as *N,N* chelating motif, and a pharmacophore unit of amino-pyrimidine that enhances the π-π conjugation and improves the stability with respect to the lead compound curcumin [38]. Indeed, the pharmacokinetic study demonstrates great stability of MPYD both in phosphate buffered saline (PBS) (data not shown) and simulated human plasma (SHP) at 37 °C (pH = 7.4) (Fig. S7, A) within 8 h, a pillar requirement in preclinical testing. These results overlay what previously observed for MPY compounds so far [23].

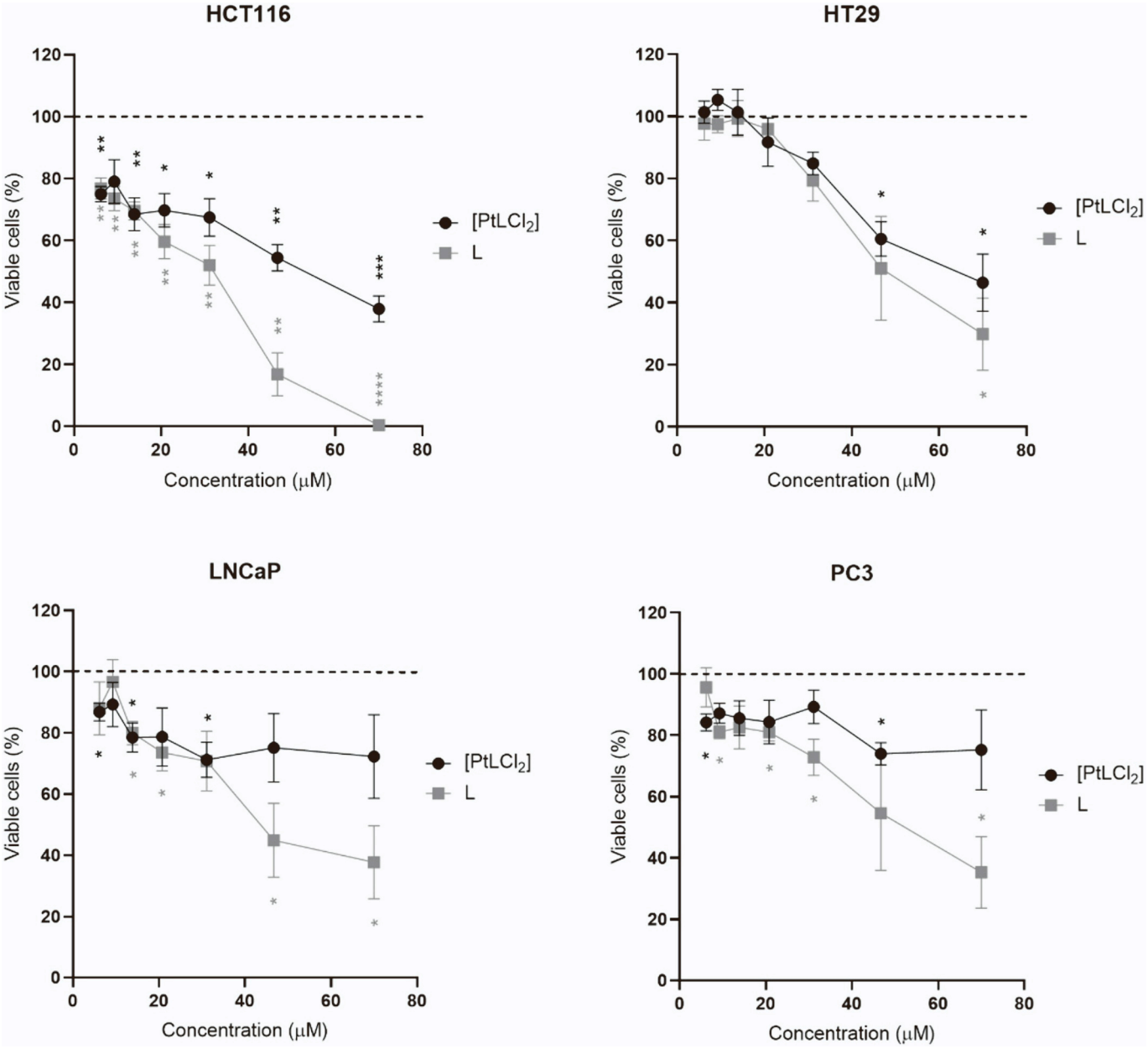

Fig. 7. Dose-dependent effect of [$PtLCl_2$] and MPYD (L) on colon (HT29 and HCT116) and prostate (LNCaP and PC3) cancer cell lines. Cell viability was assessed after 48 h of treatment with the indicated molecules dissolved in DMF in the different cell lines. Data are presented as relative percentage of viable cells (%) following [$PtLCl_2$] and MPYD (L) *versus* DMF control cells, arbitrarily set at 100% (dashed line). Graphs represent means ± standard errors of the mean (SEM), n = 3. Significance levels compared to DMF treated cells are reported as $p < 0.05$ (*), $p < 0.01$ (**), $p < 0.001$(***) and $p < 0.0001$ (****).

Table 4
IC_{50} values of [$PtLCl_2$] and MPYD (L) determined by PrestoBlue assay on colon (HT29 and HCT116) and prostate (LNCaP and PC3) cancer cell lines following 48 h from administration. IC_{50} values (μM) are indicated as means ± SEM. Data were obtained from three independent experiments. na = not active at tested concentrations.

	[$PtLCl_2$]	L	OX
HCT116	52.16 ± 3.47	31.70 ± 3.62	4.17 ± 1.34
HT29	69.58 ± 0.42	54.92 ± 10.13	16.33 ± 2.74
LNCaP	na	43.22 ± 6.21	5.85 ± 1.82
PC3	na	57.72 ± 4.01	20.74 ± 2.16

MPYD is a weak polyprotic acid and the proton dissociation equilibria are consistent with those of similar molecules [23,33]. Species distribution diagram predicts that the dominant species under physiological conditions is HL^+, with the secondary amine still protonated (Fig. 4). Complete deprotonation can be observed above pH 10, however, in presence of Pt(II) in solution, the dissociation is anticipated to form the metal complex without the addition of any base to adjust the pH. This behaviour suggests a high affinity of the ligand for Pt(II). In view of further applications, it is important to test the stability of [$PtLCl_2$] in the actual physiological conditions of the cancer microenvironment. Concerning this, intracellular and extracellular pH represent a cutting-edge topic in understanding the metabolism of cancer cells. Recently, thanks to technological advancements, it has been proven that the intracellular pH (pHi) in cancer cells is actually mildly alkaline or nearly neutral, similarly to normal cells. These findings undermine the

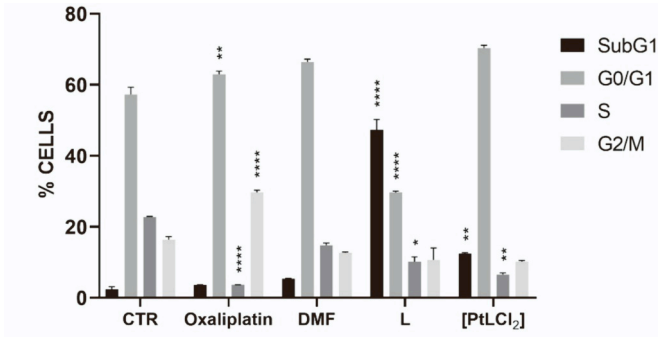

	CTR	Oxaliplatin	DMF	L	[PtLCl$_2$]
SubG1	2.4	3.6	5.3	47.3	12.5
G0/G1	57.3	63.0	66.3	29.7	70.4
S	22.8	3.7	14.8	10.2	6.6
G2/M	16.4	29.7	12.7	10.7	10.2

Fig. 8. The histogram represents the distribution of HCT116 cells in the different phases of the cell cycle following the administration of DMF, MPYD (L), [PtLCl2], and Oxaliplatin for 48 h. The values represent means ± SEM of two independent experiments. Statistical analysis was performed by matching each treatment with the corresponding solvent: Oxaliplatin was compared to CTR (complete culture medium); MPYD (L) or [PtLCl2] were compared to DMF. (two-way ANOVA with Fisher's LSD test: * $p < 0.05$, *** $p < 0.001$, **** $p < 0.0001$, $n = 2$).

given for granted assumption that the pHi in cancer cells is more acidic than normal cells. Conversely, the extracellular pH (pHe) is slightly more acidic, typically 0.3–0.7 pH unit lower than that of the corresponding normal cells. Hence, what is characteristic of tumor microenvironment is the decrease of the ratio pHe/pHi in comparison to normal tissue [39–42]. Provided this, a potential anticancer drug should be stable in the 6.5–7.6 pH range. [PtLCl$_2$] resulted extremely stable at pH 7.4, as shown by both spectroscopic and LC-MS experiments (Figs. S7 and S8). Furthermore, bearing in mind the protonation constants of the ligand, a slight decrease of the pH is not going to affect the platinum-complex stability.

NMR data allowed to investigate the formation of the Pt(II) complex *in situ*, suggesting that the reaction is quite slow at room temperature, but it can be accelerated by raising up the temperature. This method leverages the low solubility of the square planar platinum complex, allowing the isolation of the solid [PtLCl$_2$]. NMR data confirmed that the complex species present in solution by dissolving the isolated solid complex has the same spectral pattern of the one formed *in situ*. In order to unravel the structure of the complex species in solution, DFT calculations were carried out to predict the ^{1}H and ^{13}C NMR chemical shift of both the free ligand and two complex species, providing further validation of the experimental data, and to shed light on the actual structure of the Pt(II) complex in solution.

Experimental NMR chemical shifts show good correlation with the predicted DFT shieldings, with a stronger correlation observed for ^{13}C than ^{1}H (Fig. 10). Although a smaller structure (L^{C}) was used for the prediction, the results are accurate for both ^{1}H and ^{13}C. The fitting for both complexes is reasonably good, unfortunately the slight differences are not statistically significant to rule out one of the two possible structures in solution. However, mass spectrometry data (Fig. S12) support the presence in solution of the species $[PtLCl(DMSO)]^{+}$, suggesting that DMSO is able to displace only one chloride anion from the square planar coordination sphere of Pt(II). The displacement of the second chloride could possibly be prevented by the bulky ligand that hinder the formation of penta-coordinated transition state *via* associative mechanism, as notably proposed by Corinti et al. [43] for Cisplatin. The slow formation of the Pt(II) complex with MPYD in DMSO solution could be due to the competition with the coordinating solvent molecule. On the other hand, when [PtLCl$_2$] is dissolved in DMSO, the exchange of chloride with DMSO, that is enhanced by the *trans* effect of amine groups, is extremely fast and not detectable by NMR experiments.

The main route of Cisplatin and OX cell uptake is passive diffusion across the cell membrane, that is possible because the metal complex has

Table 5
Amount of internalized Pt(ng) into HCT116 cancer cell line upon incubation with [PtLCl$_2$] and OX at different doses and incubation times. Values are normalized for a million of treated cells and reported as means ±SEM.

	Dose (μM)	Incubation time (h)	[Pt] (ng/10^6 cells ± SEM)
[PtLCl$_2$]	5	6	16.47 ± 0.53
[PtLCl$_2$]	20	6	64.0 ± 15.5
[PtLCl$_2$]	50	6	391.4 ± 27.1
[PtLCl$_2$]	50	48	1070 ± 207
OX	5	6	5.86 ± 0.34
OX	5	48	59.5 ± 36.7
OX	20	6	6.98 ± 0.28
OX	50	6	13.26 ± 1.11

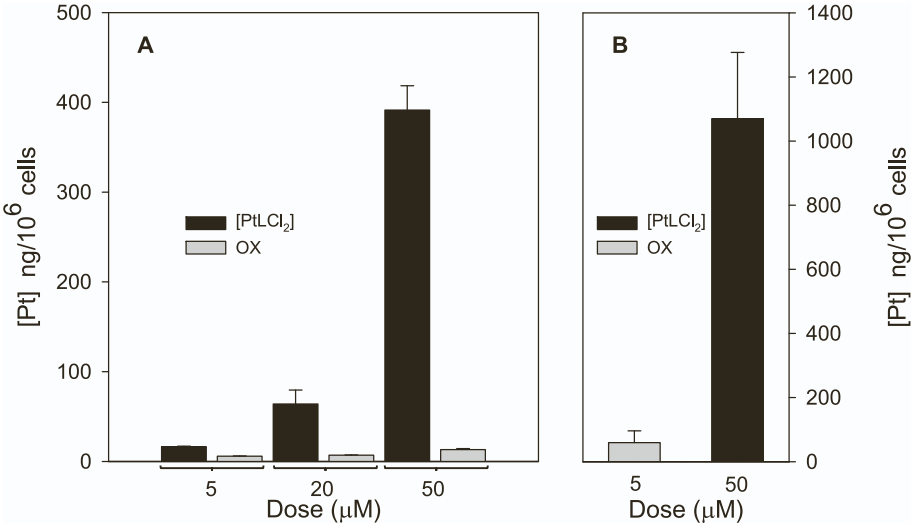

Fig. 9. Comparison of internalized Pt in HCT116 cells. (A) after 6 h incubation with [PtLCl$_2$] (black bars) and OX (grey bars) at different dosages: 5, 20 and 50 μM; (B) after 48 h incubation with [PtLCl$_2$] (black bars) and OX (grey bars) at dosages close to IC_{50}, 50 μM and 5 mM, respectively for [PtLCl$_2$] and OX. The amount of internalized Pt(ng) is normalized for a million of treated cells. Values are indicated as means ± SEM (vertical bar).

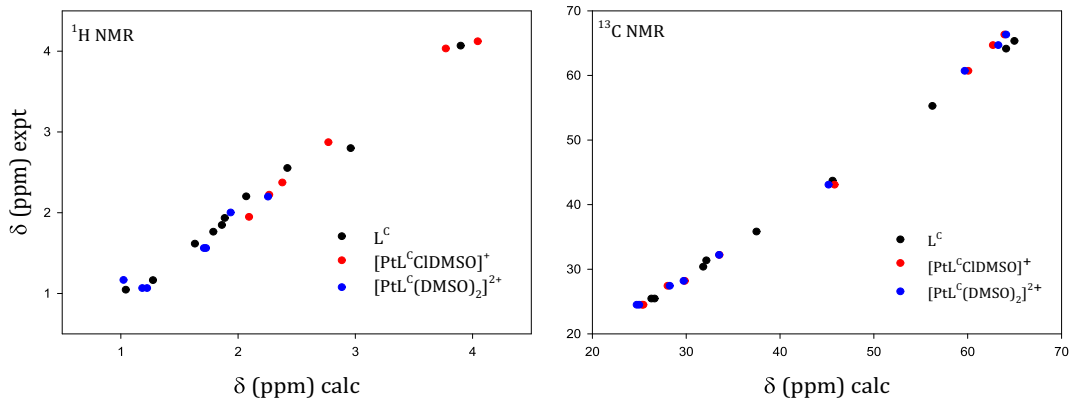

Fig. 10. Experimental *vs.* calculated ^{1}H and ^{13}C chemical shifts for L *vs.* L^C (black), the experimentally isolated platinum complex *vs.* [PtL^{C}ClDMSO]$^+$ (red) and [PtL^C(DMSO)$_2$]$^{2+}$ (blue). Linear regression was used to fit the data. (For interpretation of the references to colour in this figure legend, the reader is referred to the web version of this article.)

a zero-net charge. Indeed, the high chloride concentration (>100 mM) in the medium surrounding the cell prevents the aquation reaction that can only take place within the cytoplasm where chloride concentration is extremely lower (< 4 mM) [44]. The highly π- conjugated structure of MPY moiety may favour passive diffusion as pointed out by the higher internalization observed for [PtLCl$_2$] in comparison to OX at the same dosage. Despite the higher cellular internalization, [PtLCl$_2$] showed a weaker cytotoxicity than OX, and even lower than the free ligand. On one side the lipophilicity of MPY moiety could enhance the cellular internalization, on the other side, the high flexibility of the propyl chain may account for the folding of the ligand structure in proximity of the platinum coordination sphere. Thus, the steric hindrance and hydrophobic character of the folded ligand may slow down or even prevent the aquation reaction within the cytoplasm and consequently the interaction of the aquo-platinum complex with the DNA.

4. Conclusions

Low selectivity, drug resistance, and adverse effects caused by long-term use are just a few of the numerous challenges in the clinical use of Pt(II) class of metallo-antitumor medicines. Current research lines for Pt-based drugs have made significant advances, with a focus on structural modifications or delivery. The addition of substituents to Pt-based drugs, as well as conjugation with other chemical structures, may improve the drug's therapeutic effect through enhanced activity on DNA or additional therapeutic effects mediated by the substituents. The newly designed *N,N*-chelator (MPYD, L), which bridges DACH with amino-pyrimidine hemicurcumin has been successfully synthesized and completely characterized. MPYD exhibits enhanced stability under physiological conditions compared to the lead compound curcumin. The DACH chelating site effectively binds Pt(II) forming a 1:1 metal-to-ligand complex. Due to the low solubility of the isolated solid [PtLCl$_2$] in aqueous media, the complex formation was investigated in DMF and DMSO by ^{1}H and ^{13}C NMR spectroscopy. The complex formation kinetic in both solvents is quite slow at room temperature. Through DFT calculations and MS data, we demonstrated that a coordinating DMSO molecule can replace one chloride anion in Pt(II) square planar coordination sphere. Despite promising cellular uptake, [PtLCl$_2$] showed anticancer efficacy at higher concentration than the well-known third-generation platinum-based medication oxaliplatin after 48 and 72 h of treatment. Nevertheless, cell cycle arrest was observed after 48 h of treatment with Oxaliplatin in CRC cells, while a slight increase of cell death was induced by [PtLCl$_2$] treatment. Differences in the molecular mechanisms underlying the antiproliferative effect of [PtLCl$_2$] *versus* Oxaliplatin could account for this seemingly conflicting behaviour. Hence, the combination of DACH with the stable amino-pyrimidine hemicurcumin moiety could serve as a promising structure for the development of new Pt-based cancer treatments. Since the flexible propyl linker connecting DACH and MPY may account for the reduced antiproliferative activity, to address this issue the introduction of a rigid linker will be pursued. On the whole our findings pave the way for a more thorough pharmacological evaluation and optimisation of the new generation platinum-based drugs.

5. Material and methods

All the chemicals and solvents were purchased with the highest purity grade available and used without further purification unless otherwise specified. pH measurements were carried out using a calibrated pH-meter (Mettler-Toledo). UV–Visible spectra were acquired using a JASCO V-770 UV/Vis/NIR spectrophotometer at 25 °C in the 250–600 nm spectral range employing quartz cells (1 cm optical path). Liquid chromatography/mass spectrometry (LC/MS) was performed on an Agilent 6300 Ion Trap LC/MS system equipped with an electrospray ionization (ESI) interface. Elemental analysis was performed on a Thermo Scientific™ FLASH 2000 CHNS Analyzer. Nuclear Magnetic Resonance (NMR) spectra were recorded on a Bruker Biospin FT-NMR AVANCE III HD (600 MHz) spectrometer equipped with a CryoProbe BBO H&F 5 mm in inverse detection. The nominal frequencies were 150.90 MHz for ^{13}C and 600.13 MHz for ^{1}H, respectively. Atom numbering of NMR data refers to Fig. 1. NMR spectra were acquired in $CDCl_3$, MeOD-d_4, DMSO-d_6 and DMF-d_7 depending on the compound solubility and type of investigation.

All the reaction intermediates were purified as specified in the following procedures and their purity (≥9 5%) was checked by a combination of LC/MS, NMR and elemental analysis.

5.1. Synthesis

5.1.1. 4-(2-(2-Amino-6-methylpyrimidin-4-yl)vinyl)-2-methoxyphenol (**MPY, 1**) was prepared according to our previously published procedure (**1**)

*5.1.1.1. 4-(4-(3-Bromopropoxy)-3-methoxystyryl)-6-methylpyrimidin-2-amine (**2**).* MPY (1.227 g, 4.77 mmol) was dissolved in dimethylformamide (DMF) (3 mL), Cs_2CO_3 was added to the flask and kept under magnetic stirring. The reaction mixture turned immediately from orange to brown. After the addition of 1,3-dibromopropane (3.864 g, 19.14 mmol), the reaction was maintained under continuous stirring for 24 h in inert (Ar) atmosphere. The reaction was monitored *via* silica TLC (ethyl acetate (EtOAc):methanol (MeOH) 98:2 *V/V*). The final reaction mixture (brown-green coloured) was filtered off and the solid washed with acetone. The organic phases were collected, and the solvents were removed under reduced pressure with a rotary evaporator, giving a

greenish gluey crude product. The crude was purified by recrystallization from ethanol (EtOH) and water (75:25 *V/V* ratio) to give a yellow solid. Yield: 65%. Elemental analysis for $C_{17}H_{20}BrN_3O_2$ (378.27 g/mol).: *calc.* C(53.98%), H(5.33%), N(11.11%), *expt.* C(53.84%), H(5.37%), N (10.95%). ESI-LC/MS: 378.0 *m/z* $[M + H]^+$.

^{1}H NMR (δ (ppm); MeOD-d_4): 2.34 (H-1, s, 3H), 2.34 (H-16, *m*, J = 6.0 Hz, 2H), 3.68 (H-17, t, J = 6.53 Hz, 2H), 3.92 (H-14, s, 3H), 4.19 (H-15, t, J = 5.9 Hz, 2H), 6.72 (H-3, s, 1H), 6.88 (H-6, d, J = 16.0 Hz, 1H), 7.01 (H-10, d, J = 8.36 Hz, 1H), 7.17 (H-9, *dd*, J = 8.4 Hz, 1.9 Hz, 1H), 7.26 (H-13, d, J = 1.9 Hz, 1H), 7.69 (H-7, d, J = 16.0 Hz, 1H). ^{13}C NMR (δ (ppm); MeOD-d_4): 22.17 (C-1), 29.24 (C-17), 32.18 (C-16), 55.24 (C-14), 66.52 (C-15), 107.57 (C-3), 110.15 (C-13), 113.27 (C-10), 121.42 (C-9), 123.73 (C-6), 136.36 (C-7).

5.1.1.2. Tert-butyl ((1R,2R)-2-aminocyclohexyl)carbamate ***(3)***. The synthesis was performed according to the literature [5]. (1*R*,2*R*)-Cyclohexane-1,2-diamine (DACH, 2.01694 g, 17.66 mmol) was dissolved in 10 mL of ice-cooled dichloromethane (DCM). After 15 min, a solution of di-*tert*-butyl dicarbonate (Boc_2O, 1.35 mL, 5.89 mmol) in DCM (10 mL) was added dropwise under continuous stirring over a period of 30 min keeping the mixture cool by an ice-bath. The clear-colourless DACH solution turned white and cloudy after the addition, the temperature was risen up to room temperature and the reaction stirred overnight. Finally, 10 mL of DCM and 8 mL of water were added. The organic phase was separated, dried under Na_2SO_4 and the organic solvent was eliminated under reduced pressure by rotary evaporator. The gluey crude product was suspended in 10 mL of water, the pH was set below 5 with HCl 4 M. The mixture was extracted with diethyl ether (Et_2O) (3 × 10 mL) to remove the bis-Boc by-products. The aqueous phase was basified to pH ~10–11 with NaOH 2 M and extracted with EtOAc (4 × 12 mL). The organic phase was dried over $MgSO_4$, and the solvent was removed by rotary evaporator, giving a light-yellow solid. Yield: 72.3%.

Elemental analysis for $C_{11}H_{22}N_2O_2$ (214.31 g/mol): *calc.* C (61.65%), H (10.35%), N (13.07%), *expt.* C (61.84%), H (10.60%), N (13.19%). ESI-LC/MS: 215.1 *m/z* $[M + H]^+$.

^{1}H NMR (δ (ppm); DMSO-d_6): 1.03 (H-3/H-6, *m*, 2H), 1.14 (H-4/H-5, *m*, 2H), 1.38 (H-9, s, 9H), 1.58 (H-4'/H-5′, *m*, 2H), 1.75 (H-3'/H-6′, m, 2H), 2.31 (H-1, *m*, 1H), 2.88 (H-2, m, 1H), 6.63 (CHN<u>H</u>CO, 1H). ^{13}C NMR (δ (ppm); DMSO-d_6): 24.69, 24.86 (C-4/C-5), 28.28 (C-9), 32.08, 34.44 (C-3/C-6), 53.74 (C-1), 57.02 (C-2), 77.3 (C-8), 155.6 (C-7).

5.1.1.3. Tert-butyl ((1R,2R)-2-((3-(4-(2-(2-amino-6-methylpyrimidin-4-yl)vinyl)-2-methoxyphenoxy) propyl)amino)cyclohexyl)carbamate ***(4)***. Cs_2CO_3 (0.38862 g, 1.19 mmol) was suspended in 3 mL of anhydrous DMF, stirred under Ar atmosphere, then **3** (0.17188 g, 0.80 mmol) was added to the reaction flask. A solution of **2** (0.30020 g, 0.79 mmol) in anhydrous DMF (3 mL) was slowly dropped into the reaction mixture that rapidly turned light brown. The reaction was maintained under stirring in inert atmosphere (Ar) at room temperature for 24 h, then the temperature was risen up to 50 °C and stirring was continued for 24 h. The solid was filtered off. The solvent, dried under $MgSO_4$, was then removed by rotary evaporator. The product was purified by silica flash-chromatography (gradient EtOAc:MeOH from 100:0 to 80:20 *V/V*), obtaining a brown solid. Yield: 41.0%. Elemental analysis for $C_{28}H_{41}N_5O_4$ (511.67 g/mol): *calc.* C(65.73%), H(8.08%), N(13.69%), *expt.* C(65.24%), H(8.37%), N(13.97%). ESI-LC/MS: 512.1 *m/z* $[M + H]^+$. ^{1}H NMR (δ (ppm); MeOD-d_4): 1.31(H-20/H-21/H-22/H-23, *m*, 4H), 1.37 (H-26, s, 9H), 1.77 (H-21'/H-22′, *m*, 2H), 1.95 (H-20′, *m*, 1H), 2.05 (H-16, *m*, 2H), 2.10 (H-23′, *m*, 1H), 2.35 (H-1, s, 3H), 2.57 (H-18, *m*, 1H), 2.89 (H-17, *m*, 1H), 3.04 (H-17′, *m*, 1H), 3.37 (H-19, *m*, 1H), 3.93 (H-14, s, 3H), 4.13 (H-15, *m*, 2H), 6.72 (H-3, s, 1H), 6.88 (H-6, d, J = 16 Hz 1H), 7.01 (H-10, d, J = 8.3 Hz, 1H), 7.17 (H-9, *dd*, 1H), 7.27 (H-13, d, J = 1.8 Hz, 1H), 7.70 (H-7, d, J = 16.0 Hz, 1H). ^{13}C NMR (δ (ppm); MeOD-d_4): 22.14 (C-1), 24.10, 24.61 (C-21, C-22), 27.29 (C-26), 27.93 (C-16), 29.57 (C-23), 32.26 (C-20), 43.11 (C-17), 53.03 (C-19), 55.15 (C-14), 60.26 (C-18), 67.69 (C-15), 107.53 (C-3), 109.96 (C-13), 113.29 (C-10), 121.41 (C-9), 123.76 (C-6), 136.27 (C-7).

5.1.1.4. (1R,2R)-N1-(3-(4-((E)-2-(2-Amino-6-methylpyrimidin-4-yl) vinyl)-2-methoxyphenoxy) propyl) cyclohexane-1,2-diamine ***(MPYD, L, 5)***. **4** (103.95 mg, 0.2032 mmol) was dissolved in 3 mL DCM and trifluoroacetic acid (TFA, 1 mL) was then added. The solution turned from yellow orange to dark red. The reaction mixture was sonicated for 90 min at RT. The solvent was then evaporated by rotary evaporator and the obtained product dissolved in 3 mL DCM. The DCM was then removed (3 cycles of DCM solubilization – evaporation). The final product was dissolved in water (2 mL) and precipitated by the addition of NaOH 2 M. The solid was isolated by centrifugation and dried under vacuum, giving a brown-yellow solid. Yield: 50%.

Elemental analysis for $C_{23}H_{33}N_5O_2$ (411.55 g/mol): *calc.* C (67.12%), H (8.08%), N (17.02%), *expt.* C (66.98%), H (7.98%), N (17.21%). ESI-LC/MS: 412.1 *m/z* $[M + H]^+$. ^{1}H NMR (δ (ppm); MeOD-d_4): 1.06 (H-23, m, 1H), 1.20 (H-20, m, 1H), 1.29 (H-21/H22, m, 2H), 1.73 (H-21'/H22', m, 2H), 1.92 (H-20′, m, 1H), 2.01 (H-16, qt, J = 6.3 Hz, 2H), 2.08 (H-23′, m, 1H), 2.17 (H-18, m, 1H), 2.32 (H-1, s, 3H), 2.43 (H-19, m, 1H), 2.71 (H-17, m, 1H), 2.98 (H-17′, m, 1H), 3.90 (H-14, s, 3H), 4.15 (H-15, t, J = 5.5 Hz, 2H), 6.70 (H-3, s, 1H), 6.85 (H-6, d, J = 16.0 Hz, 1H), 6.98 (H-10, d, J = 8.6 Hz, 1H), 7.15 (H-9, dd, J = 8.4 Hz, 1H), 7.24 (H-13, d, J = 1.9 Hz, 1H), 7.68 (H-7, d, J = 16.0 Hz, 1H). ^{13}C NMR (δ (ppm); MeOD-d_4): 23.60 (C-1), 26.14 (C-21, C-22), 30.32 (C-16), 31.55 (C-23), 35.23 (C-20), 45.30 (C-17), 55.70 (C-19), 56.50 (C-14), 64.43 (C-18), 69.06 (C-15), 108.92 (C-3), 111.27 (C-13), 114.03 (C-10), 122.89 (C-9), 124.8 (C-6), 137.76 (C-7).

5.1.1.5. Dichloro((1R,2R)-N1-(3-(4-((E)-2-(2-amino-6-methylpyrimidin-4-yl)vinyl)-2-methoxyphenoxy) propyl) cyclohexane-1,2-diamine)platinum (II) [PtLCl$_2$] ***(6)***. The following synthesis is a modification of previously reported syntheses of similar Pt(II) complexes [9–12]. A solution of **5** (12.99 mg, 0.0316 mmol) in EtOH (1 mL) was dropped to a K_2PtCl_4 aqueous solution (15.08 mg/mL, 0.0363 mmol/mL) under magnetic stirring. The reaction mixture was stirred for 24 h in the darkness at RT, and it turned slowly from light-red to yellow-orange. The reaction mixture was centrifuged and the solvent was removed. The solid was then washed with cold H_2O (2 × 1 mL), cold EtOH (2 × 1 mL) and Et_2O (2 × 1 mL), removing every time the solvent after centrifugation. Finally, the yellow solid was dried under vacuum. Yield: 86%. Elemental analysis for $C_{23}H_{33}N_5O_2Cl_2Pt$ (677.53 g/mol): *calc.* C (40.77%), H (4.91%), N (10.34%), *expt.* C (40.66%), H(4.85), N (10.23%). ESI-LC/MS: 677.17 *m/z* $[M + H]^+$. ^{1}H NMR (δ (ppm); DMF-d_7): 1.19 (H-21, H-22, m, 2H), 1.37 (H-23, m, 1H), 1.51 (H-20, m, 1H), 1.63 (H-21′, H-22′, m, 2H), 2.18 (H-20′, m, 1H), 2.32 (H-16, m, 1H), 2.37 (H-23′, m, 1H), 2.38 (H-1, s, 3H), 2.49 (H-18, m, 1H), 2.59 (H-19, m, 1H), 2.83 (H-16′, m, 1H), 2.86 (H-17, m, 1H), 3.40 (H-17′, m, 1H), 3.96 (H-14, s, 3H), 4.13 (H-15, m, 1H), 4.31 (H-15′, m, 1H), 5.16 (CHN<u>H$_2$</u>, t, J = 10.4 Hz, 1H), 5.61 (CHN<u>H$_2$</u>, d, J = 7.0 Hz, 1H), 6.18 (CH$_2$N<u>H</u>CH, d, J = 10.0 Hz, 1H), 6.81 (H-3, s, 1H), 7.09 (H-6, d, J = 16.0 Hz, 1H), 7.13 (H-10, d, J = 8.5 Hz, 1H), 7.26 (H-9, dd, J = 8.4 Hz, 1.7 Hz, 1H), 7.44 (H-13, d, 1.7 Hz, 1H), 7.88 (H-7, d, J = 16.0 Hz, 1H). ^{13}C NMR (δ (ppm) DMF-d_7): 22.16 (C-1), 24.53 (C-22), 24.77 (C-21), 27.21 (C-16), 28.09 (C-23), 32.18 (C-20), 43.48 (C-17), 55.59 (C-14), 62.46 (C-19), 66.10 (C-18), 66.54 (C-15), 107.65 (C-3), 110.33 (C-13), 112.97 (C-10), 122.24 (C-15).

5.2. Spectrophotometric pH-titrations

Spectrophotometric pH-titrations were performed on MPY-DACH following the procedure previously reported for the lead compound MPY and its derivatives [23]. Briefly, MPYD (denoted generally as L in the following) was dissolved in methanol and then diluted in water to the final concentration of 20 μM (MeOH <3% *V/V*). 25 mL of the

solution were analysed. The pH was varied by adding small amounts (1 μL) of concentrated NaOH/HCl (4 M) in order to investigate the spectral behaviour in the 2–11 pH range. In these conditions volume variations are negligible. The titration was performed in triplicate. A constant ionic strength ($NaNO_3$, 0.1 M) was maintained in all the experiments.

β_{qr} values were refined from spectrophotometric data using least-squares calculation in HypSpec [32]. The results of least-squares calculations include the standard deviations and correlation coefficients of the refined parameters. The quantities are obtained by performing error propagation calculations from the experimental errors onto the parameters. The stability constant refinement furnishes least-squares estimates of the standard deviation, σ, of the stability constant β. The error on logβ is calculated as follows: $\sigma(\log\beta) = [\log(\beta + \sigma) - \log(\beta - \sigma)]/2$.

5.3. Complexation studies with Pt(II) by NMR

The complexation studies of **5** with Pt(II) were performed in NMR test tube at 25 °C, both in DMSO-d_6 and DMF-d_7. The procedure used for the study is the following. A solution in the deuterated solvent of **5** (3.00 mg in 750 μL of DMSO-d_6; 5.47 mg in 750 μL of DMF-d_7) was prepared and then 1 equivalent of K_2PtCl_4 147.7 mM in D_2O (49 μL for DMSO-d_6 solution; 86 μL for DMF-d_7 solution) was added in order to reach a metal: ligand ratio of 1:1. The spectra were acquired at different time intervals in order to follow the kinetics of complexation.

5.4. Computational details for NMR chemical shift simulations

In order to tune and assess a viable computational approach, experimental reference values for NMR chemical shifts (δ) were obtained from literature [45,46], comprising experimental values for 66 organic compounds in a few commonly used solvents, including DMSO. These include 590 hydrogen and 291 carbon atoms, corresponding to 155 ^{1}H and 190 ^{13}C NMR signals useful for fitting. All computations were performed using Gaussian09 [47] or Gaussian16 [48] with SCRF implicit solvation with the dielectric parameters for DMSO, namely $\varepsilon = 46.515$ [49] and $\varepsilon\infty = 2.1904$, obtained from the square of the refractive index [50]. Following the approach proposed in literature [51–53] different levels of theory were tested to compute geometries and NMR shieldings. The method and basis sets used are reported in Table S4, along with their usage (geometry optimization or NMR response) and short labels. These were then combined to indicate the method used to compute NMR shieldings. For instance the label G1N3 refers to B3LYP/6–31+G(d,p) geometries (level G1) and B3LYP/6–311+G(2d,p) NMR shieldings (level N3). The computed ^{1}H NMR shiedings (σ) were plotted against the experimental chemical shifts and a linear least squares regression line was determined. Due to significant deviations from linearity observed for protons bound to oxygen using SCRF implicit solvation (Fig. S13) and the difficulties in adding explicit solvent molecules for the investigated systems, we decided to exclude alcoholic hydrogens from the fit. Overall results are summarized in Table S5. The slight discrepancies in the RMSE obtained with respect to data reported by Pierens et al. [52], based on gas phase geometries, may be due to a different set of training compounds. Upon these findings, the combination G1N3 was selected. For applications to the systems relevant for this investigation, Pt atoms were described with the LANL2 [54] effective core potential and corresponding basis set matching the G1 and N3 number of polarization functions. To sample the configuration space, we treated the system as follows:

i) molecular dynamics simulation based on the Universal Force Field (UFF) [55] was performed for 20 ps at 900 K, generating 20,000 structures for each of the species $[PtL^{C}Cl(DMSO)]^{+}$, $[PtL^{C}(DMSO)_2]^{2+}$, and L^{C};
ii) for each structure, the value of the internal dihedrals were measured and rounded to the nearest stable value (180°, 60°, and − 60° for ternary; 180° and 0° for binary dihedrals) and for each combination of dihedrals the geometry closest to the stable values was selected for the following step, with a reduction of the overall number of structures from 60,000 (3 · 20,000) to 163;
iii) the geometry for these configurations was optimized with a low level of quantum mechanics (B3LYP/6-31G) and only the structures with different values of rounded dihedrals were selected, resulting in 159 configurations;
iv) These were optimized at the more accurate level G1 and again only the structures with different rounded torsions were selected;
v) The probability distribution for these geometries was estimated based on Boltzmann equation for room temperature using G1 energies, and NMR shieldings were computed for structures with a probability >1% relative to the lowest energy configuration;

Specifically, NMR shieldings were computed for 10, 7, and 23 configurations for $[PtL^{C}(DMSO)_2]^{2+}$, $[PtL^{C}Cl(DMSO)]^{+}$, and L^{C}, respectively.

Shieldings for equivalent atoms were averaged and the values from all geometries were combined with Boltzmann weights to generate a simulated spectrum at room temperature. Standard deviations were obtained with standard error propagation techniques accounting for (a) the uncertainty in the interpolating coefficients, based on likelihood function formalism, and (b) the standard deviation from the Boltzmann averaging over several geometric configurations. The resulting standard deviation is consistently larger than the RMSE from the interpolating reference set, mainly due to averaging over the sampled geometric configurations.

5.5. Stability in simulated physiological conditions

The chemical stability at 37 °C in darkness was evaluated for L and $[PtLCl_2]$ by UV − Vis spectroscopy as a change in absorbance in the 250–600 nm range over a period of 8 h. 20 μM solution of L and $[PtLCl_2]$ was prepared in simulated plasma fluid (SPF) as previously reported [56] at pH 7.4. Spectra were recorded every 5 min during the first hour and every 30 min the following ones. The stability of $[PtLCl_2]$ in phosphate buffered saline (PBS, pH 7.4) was tested after 48 h of incubation at 37 °C by ESI-LC-MS.

5.6. Cell lines

The human colon cancer cell lines HT29 (ATCC Cat# HTB-38) and HCT116 (ATCC Cat# CCL-247) were grown in DMEM High-Glucose Medium (Biowest, France). The human prostate cancer cells PC3 (ATCC Cat# CRL-1435) and LNCaP (ATCC Cat# CRL-1740) were grown in Ham's F12 (Biowest, France) and RPMI 1640 (Biowest, F[14–17] rance), respectively. All media were supplemented with 10% Foetal Bovine Serum (FBS, Gibco), 2 mM L-glutamine, 100 IU/mL penicillin and 100 μg/mL streptomycin. The cells were grown at 37 °C in a humified 5% CO_2 atmosphere.

5.7. Cell viability assay

The inhibition of cellular proliferation was measured using Presto Blue cell viability reagent (#A13261, Thermo Fisher Scientific, Waltham, MA, USA), according to the manufacturer's protocol. HCT116, HT29, PC3, or LNCaP cells were seeded into a 96-well plate at a density of 4000 cells/well. Cells were treated for 48 h or 72 h with seven different concentrations of MPYD (L) dissolved in DMSO or or $[PtLCl_2]$ and L dissolved in DMF, at concentrations starting at 70 μM with 1.5-fold serial dilutions. The percentage (*V*/V) of DMSO or DMF in the final solution was below 1%. The positive control drug Oxaliplatin dissolved in H_20 (MedChemExpress, NJ, USA) was administered for 48 h or 72 h, starting at a concentration of 33.3 μM or 14.8 μM, respectively, with 1.5-fold serial dilutions. Matched serial dilutions of DMSO and DMF were included as controls; the percentage of viable cells in compound-treated

samples was normalized to the values obtained with the same amount (%, V/V) of matched solvent (DMSO or DMF, as needed), to avoid possible solvent-related biases. The concentration at which the cell population is reduced by 50% (IC_{50}) was then determined. Statistical analysis was performed using GraphPad PRISM 8 software (GraphPad Prism), using two-way ANOVA with Fisher's LSD test. Graphs represent means ± standard errors of the mean (SEM), $n = 3$. Data were statistically significant if $p < 0.05$ (*), $p < 0.01$ (**), $p < 0.001$(***), and $p < 0.0001$ (****).

5.8. Cell cycle analysis

Cells were seeded into a 24-well plate at a density of 35,000 cells/well, harvested after 48 h of treatment with Oxaliplatin, MPYD (L) or [$PtLCl_2$] at IC50 concentrations and stained with propidium iodide solution (propidium iodide 25 μg/mL, Na-Citrate 3.4 mM, NaCl 9.65 mM, NP-40 0.03%). Complete culture medium (CTR) or DMF were used as controls. Cell cycle analysis was performed using an Attune Next cytofluorimeter (Thermo Fisher Scientific, Waltham, MA, USA). Statistical analysis was performed with GraphPad PRISM 8 software (GraphPad Prism), using two-way ANOVA with Fisher's LSD test: Oxaliplatin was compared to CTR, while MPYD (L) or [$PtLCl_2$] were compared to DMF, to account for the matched-solvent of the different compounds. Graph represents means ± standard errors of the mean (SEM), $n = 2$. Data were considered to be statistically significant if $p < 0.05$ (*), $p < 0.01$ (**), $p < 0.001$(***), and $p < 0.0001$ (****).

5.9. Platinum uptake in cells

60.000 HCT116 cells were seeded into 12-well plates and treated at different dosages (5, 20, 50 μM) and incubation times (6 h and 48 h) with [$PtLCl_2$] and Oxaliplatin (OX) in DMF. The percentage of DMF (*V/V*) was kept below 1%, and the same conditions (1% V/V DMF) were used as control. After the incubation time, the cells were washed twice with PBS and cell pellets were frozen and stored at −80 °C. The cell pellets were digested for 24 h in 200 μL of ultrapure HNO_3 65% *w/w*, obtained from analytical grade nitric acid (Carlo Erba, Milan, Italy) after sub-boiling distillation performed with a sub-boiler SAVILLEX DST 1000 (Savillex Corp. USA) apparatus. The resulting solutions were diluted up to a total mass of 4 g with Milli-Q water in 15 mL polypropylene tubes and analysed for their Pt content. The collected samples were randomly acquired using the inductively coupled plasma mass spectrometer iCAP TQ ICP-MSX (Thermo Fisher Scientific) equipped with Peltier cooled (3 °C) spray chamber. Samples were introduced by the autosampler ESI SC-2 DX FAST into the nebulizer, and the positively charged ions were then produced by a high-temperature, inductively coupled plasma. Data were analysed by Qtegra software. The instrument was tuned daily with an ICP-MS tuning solution. Y in HNO_3 2% (100 ppb) was used as internal standard. Pt standard solutions ranging from 0.1 to 100 ppb were freshly prepared before each analysis and used to build the calibration curve. Two replicates of each experiment were carried out. Each sample was analysed at least in 2 independent measurements and each measurement is the average of 5 repetitions. Results are given as mean value ± standard deviation.

CRediT authorship contribution statement

Matteo Mari: Writing – original draft, Formal analysis. **Matteo Boniburini:** Formal analysis. **Marianna Tosato:** Writing – review & editing, Visualization, Data curation. **Filippo Bonini:** Formal analysis. **Francesco Faglioni:** Writing – review & editing, Writing – original draft, Investigation, Data curation. **Laura Cuoghi:** Formal analysis, Data curation. **Silvia Belluti:** Writing – review & editing, Data curation. **Carol Imbriano:** Writing – review & editing, Writing – original draft, Methodology, Data curation. **Mattia Asti:** Writing – review & editing. **Erika Ferrari:** Writing – review & editing, Writing – original draft, Supervision, Project administration, Conceptualization.

Declaration of competing interest

The authors declare that they have no known competing financial interests or personal relationships that could have appeared to influence the work reported in this paper.

Data availability

Data will be made available on request.

Acknowledgements

The Authors thank the "Centro Interdipantimentale Grandi Strumenti – C.I.G.S." on the University of Modena and Reggio Emilia (https://www.cigs.unimore.it) for the NMR, the Mass spectrometers and their precious technical support. MT acknowledges the COST NECTAR action (Network for Equilibria and Chemical Thermodynamics Advanced Research COST ACTION 18202; https://www.cost-nectar.eu) for supporting her attendance to "2023_NECTAR_Training-School on Communication in Science".

Appendix A. Supplementary data

Supplementary data to this article can be found online at https://doi.org/10.1016/j.jinorgbio.2024.112702.

References

[1] Global Cancer Observatory, (n.d.). https://gco.iarc.fr/en.
[2] G. Mauri, V. Gori, E. Bonazzina, A. Amatu, F. Tosi, K. Bencardino, L. Ruggieri, G. Patelli, S. Arena, A. Bardelli, S. Siena, A. Sartore-Bianchi, Oxaliplatin retreatment in metastatic colorectal cancer: systematic review and future research opportunities, Cancer Treat. Rev. 91 (2020) 102112, https://doi.org/10.1016/j.ctrv.2020.102112.
[3] R.J. Rebello, C. Oing, K.E. Knudsen, S. Loeb, D.C. Johnson, R.E. Reiter, S. Gillessen, T. Van der Kwast, R.G. Bristow, Prostate cancer, Nat. Rev. Dis. Prim. 7 (2021), https://doi.org/10.1038/s41572-020-00243-0.
[4] B. Cevatemre, I. Bulut, B. Dedeoglu, A. Isiklar, H. Syed, O.Y. Bayram, T. Bagci-Onder, C. Acilan, Exploiting epigenetic targets to overcome taxane resistance in prostate cancer, Cell Death Dis. 15 (2024), https://doi.org/10.1038/s41419-024-06422-1.
[5] S. Hager, C.J. Ackermann, M. Joerger, S. Gillessen, A. Omlin, Anti-tumour activity of platinum compounds in advanced prostate cancer-a systematic literature review, Ann. Oncol. 27 (2016) 975–984, https://doi.org/10.1093/annonc/mdw156.
[6] S. Schmid, A. Omlin, C. Higano, C. Sweeney, N. Martinez Chanza, N. Mehra, M.C. P. Kuppen, H. Beltran, V. Condeduca, D. Vargas Pivato De Almeida, F. Cotait Maluf, W.K. Oh, C.K. Tsao, O. Sartor, E. Ledet, G. Di Lorenzo, S.M. Yip, K.N. Chi, D. Bianchini, U. De Giorgi, A.R. Hansen, T.M. Beer, L. Pernelle, R. Morales-Barrera, M. Tucci, E. Castro, K. Karalis, A.M. Bergman, M.L. Le, U. Zürrer-Härdi, C. Pezaro, H. Suzuki, A. Zivi, D. Klingbiel, S. Schär, S. Gillessen, Activity of platinum-based chemotherapy in patients with advanced prostate Cancer with and without DNA repair gene aberrations, JAMA Netw. Open 3 (2020) 1–15, https://doi.org/10.1001/jamanetworkopen.2020.21692.
[7] M. Catalano, A. Lapucci, S. Nobili, I. De Gennaro Aquino, I.A. Vascotto, L. Antonuzzo, D. Villari, G. Nesi, E. Mini, G. Roviello, Platinum-based chemotherapy in metastatic prostate cancer: what possibilities? Cancer Chemother. Pharmacol. 93 (2024) 1–9, https://doi.org/10.1007/s00280-023-04604-w.
[8] L. Bai, C. Gao, Q. Liu, C. Yu, Z. Zhang, L. Cai, B. Yang, Y. Qian, J. Yang, X. Liao, Research progress in modern structure of platinum complexes, Eur. J. Med. Chem. 140 (2017) 349–382, https://doi.org/10.1016/j.ejmech.2017.09.034.
[9] M. Shahlaei, S.M. Asl, A. Derakhshani, L. Kurek, J. Karges, R. Macgregor, M. Saeidifar, I. Kostova, A.A. Saboury, Platinum-based drugs in cancer treatment: expanding horizons and overcoming resistance, J. Mol. Struct. 1301 (2024) 137366, https://doi.org/10.1016/j.molstruc.2023.137366.
[10] C. Zhang, C. Xu, X. Gao, Q. Yao, Platinum-based drugs for cancer therapy and anti-tumor strategies, Theranostics 12 (2022) 2115–2132, https://doi.org/10.7150/thno.69424.
[11] P.M. Bruno, Y. Liu, G.Y. Park, J. Murai, C.E. Koch, T.J. Eisen, J.R. Pritchard, Y. Pommier, S.J. Lippard, M.T. Hemann, A subset of platinum-containing chemotherapeutic agents kills cells by inducing ribosome biogenesis stress, Nat. Med. 23 (2017) 461–471, https://doi.org/10.1038/nm.4291.
[12] N. Summa, T. Soldatović, L. Dahlenburg, Ž.D. Bugarčić, R. Van Eldik, The impact of different chelating leaving groups on the substitution kinetics of mononuclear PtII (1,2-trans-R,R-diaminocyclohexane)(X-Y) complexes, J. Biol. Inorg. Chem. 12 (2007) 461–475, https://doi.org/10.1007/s00775-006-0200-z.

[13] N. Summa, W. Schiessl, R. Puchta, N. Van Eikema Hommes, R. Van Eldik, Thermodynamic and kinetic studies on reactions of Pt(II) complexes with biologically relevant nucleophiles, Inorg. Chem. 45 (2006) 2948–2959, https://doi.org/10.1021/ic051955r.
[14] V. Basile, E. Ferrari, S. Lazzari, S. Belluti, F. Pignedoli, C. Imbriano, Curcumin derivatives: molecular basis of their anti-cancer activity, Biochem. Pharmacol. 78 (2009) 1305–1315, https://doi.org/10.1016/J.BCP.2009.06.105.
[15] E. Ferrari, S. Lazzari, G. Marverti, F. Pignedoli, F. Spagnolo, M. Saladini, Synthesis, cytotoxic and combined cDDP activity of new stable curcumin derivatives, bioorganic, Med. Chem. 17 (2009) 3043–3052, https://doi.org/10.1016/j.bmc.2009.03.016.
[16] K.M. Nelson, J.L. Dahlin, J. Bisson, J. Graham, G.F. Pauli, M.A. Walters, The essential medicinal chemistry of curcumin, J. Med. Chem. 60 (2017) 1620–1637, https://doi.org/10.1021/acs.jmedchem.6b00975.
[17] O.A. Ojo, T.R. Adeyemo, D. Rotimi, G.E.S. Batiha, G. Mostafa-Hedeab, M. E. Iyobhebhe, T.C. Elebiyo, B. Atunwa, A.B. Ojo, C.M.G. Lima, C.A. Conte-Junior, Anticancer properties of curcumin against colorectal cancer: a review, Front. Oncol. 12 (2022) 1–13, https://doi.org/10.3389/fonc.2022.881641.
[18] C. Liu, M. Rokavec, Z. Huang, H. Hermeking, Curcumin activates a ROS/KEAP1/NRF2/miR-34a/b/c cascade to suppress colorectal cancer metastasis, Cell Death Differ. (2023), https://doi.org/10.1038/s41418-023-01178-1.
[19] D. Termini, D.J. Den Hartogh, A. Jaglanian, E. Tsiani, Curcumin Against Prostate Cancer: Current Evidence, 2020, https://doi.org/10.3390/biom10111536.
[20] T.H. Marczylo, R.D. Verschoyle, D.N. Cooke, P. Morazzoni, W.P. Steward, A. J. Gescher, Comparison of systemic availability of curcumin with that of curcumin formulated with phosphatidylcholine, Cancer Chemother. Pharmacol. 60 (2007) 171–177, https://doi.org/10.1007/s00280-006-0355-x.
[21] A.N. Begum, M.R. Jones, G.P. Lim, T. Morihara, P. Kim, D.D. Heath, C.L. Rock, M. A. Pruitt, F. Yang, B. Hudspeth, S. Hu, K.F. Faull, B. Teter, G.M. Cole, S. A. Frautschy, Curcumin structure-function, bioavailability, and efficacy in models of neuroinflammation and Alzheimer's disease, J. Pharmacol. Exp. Ther. 326 (2008) 196–208, https://doi.org/10.1124/jpet.108.137455.
[22] V.K. Rapalli, V. Kaul, S. Gorantla, T. Waghule, S.K. Dubey, M.M. Pandey, G. Singhvi, UV spectrophotometric method for characterization of curcumin loaded nanostructured lipid nanocarriers in simulated conditions: method development, in-vitro and ex-vivo applications in topical delivery, Spectrochim, Acta - Part A Mol. Biomol. Spectrosc. 224 (2020) 117392, https://doi.org/10.1016/j.saa.2019.117392.
[23] M. Mari, M. Boniburini, M. Tosato, L. Rigamonti, L. Cuoghi, S. Belluti, C. Imbriano, G. Avino, M. Asti, E. Ferrari, Development of stable amino-pyrimidine–curcumin analogs: synthesis, equilibria in solution, and potential anti-proliferative activity, Int. J. Mol. Sci. 24 (2023) 13963, https://doi.org/10.3390/ijms241813963.
[24] J.P. Parrish, B. Sudaresan, K.W. Jung, Improved Cs2CO3 promoted O-alkylation of phenols, Synth. Commun. 29 (1999) 4423–4431, https://doi.org/10.1080/00397919908086606.
[25] R.N. Salvatore, A.S. Nagle, W.J. Kyung, Cesium effect: high chemoselectivity in direct N-alkylation of amines, J. Organomet. Chem. 67 (2002) 674–683, https://doi.org/10.1021/jo010643c.
[26] R.N. Salvatore, A.S. Nagle, S.E. Schmidt, K.W. Jung, Cesium hydroxide promoted chemoselective N-alkylation for the generally efficient synthesis of secondary amines, Org. Lett. 1 (1999) 1893–1896, https://doi.org/10.1021/ol9910417.
[27] P. Lagriffoule, P. Wittung, M. Eriksson, K.K. Jensen, B. Nordén, O. Buchardt, P. E. Nielsen, Peptide nucleic acids with a conformationally constrained chiral cyclohexyl-derived backbone, Chem. - A Eur. J. 3 (1997) 912–919, https://doi.org/10.1002/chem.19970030613.
[28] J.J. Wilson, S.J. Lippard, Synthetic methods for the preparation of platinum anticancer complexes, Chem. Rev. 114 (2014) 4470–4495, https://doi.org/10.1021/cr4004314.
[29] J. De Mier-Vinué, M. Gay, Á.M. Montaña, R.I. Sáez, V. Moreno, J. Kasparkova, O. Vrana, P. Heringova, V. Brabec, A. Boccarelli, M. Coluccia, G. Natile, Synthesis, biophysical studies, and antiproliferative activity of platinum(II) complexes having 1,2-bis(aminomethyl)carbobicyclic ligands, J. Med. Chem. 51 (2008) 424–431, https://doi.org/10.1021/jm070844u.
[30] A. Bacchi, M. Carcelli, P. Pelagatti, G. Rispoli, D. Rogolino, Supramolecular architectures of Pt(II) complexes controlled by hydrogen bonds and by guest molecules, Cryst. Growth Des. 12 (2012) 387–396, https://doi.org/10.1021/cg201185c.
[31] P. Štarha, J. Marek, Z. Trávníček, Cisplatin and oxaliplatin derivatives involving 7-azaindole: structural characterisations, Polyhedron 33 (2012) 404–409, https://doi.org/10.1016/j.poly.2011.11.059.
[32] P. Gans, A. Sabatini, A. Vacca, To improve accuracy of the calculated pKa values, Ann. Chim. 89 (1999) 45–49.
[33] S. Evjen, I.R. Krokvik, A. Fiksahl, H. Knuutila, Analysis of the protonation constant (pKa) and absorption properties of non-alkanolamines, Energy Procedia 114 (2017) 2590–2598, https://doi.org/10.1016/j.egypro.2017.03.1416.
[34] L. Castellino, E. Alladio, S. Bertinetti, G. Lando, C. De Stefano, S. Blasco, E. García-España, S. Gama, S. Berto, D. Milea, PyES – an open-source software for the computation of solution and precipitation equilibria, Chemom. Intell. Lab. Syst. 239 (2023), https://doi.org/10.1016/j.chemolab.2023.104860.
[35] F.D. Rochon, A. Morneau, 195Pt and 1H NMR studies of platinum(II) complexes with ethylenediamine derivatives, Magn. Reson. Chem. 29 (1991) 120–126, https://doi.org/10.1002/mrc.1260290205.
[36] M.D. Hall, K.A. Telma, K.E. Chang, T.D. Lee, J.P. Madigan, J.R. Lloyd, I.S. Goldlust, J.D. Hoeschele, M.M. Gottesman, Say no to DMSO: dimethylsulfoxide inactivates cisplatin, carboplatin, and other platinum complexes, Cancer Res. 74 (2014) 3913–3922, https://doi.org/10.1158/0008-5472.CAN-14-0247.
[37] D. Arango, A.J. Wilson, Q. Shi, G.A. Corner, M.J. Arañes, C. Nicholas, M. Lesser, J. M. Mariadason, L.H. Augenlicht, Molecular mechanisms of action and prediction of response to oxaliplatin in colorectal cancer cells, Br. J. Cancer 91 (2004) 1931–1946, https://doi.org/10.1038/sj.bjc.6602215.
[38] Y.J. Wang, M.H. Pan, A.L. Cheng, L.I. Lin, Y.S. Ho, C.Y. Hsieh, J.K. Lin, Stability of curcumin in buffer solutions and characterization of its degradation products, J. Pharm. Biomed. Anal. 15 (1997) 1867–1876, https://doi.org/10.1016/S0731-7085(96)02024-9.
[39] J. Michl, S. Monterisi, B. White, W. Blaszczak, A. Hulikova, G. Abdullayeva, E. Bridges, Z. Yin, W.F. Bodmer, P. Swietach, Acid-adapted cancer cells alkalinize their cytoplasm by degrading the acid-loading membrane transporter anion exchanger 2, SLC4A2, Cell Rep. 42 (2023) 112601, https://doi.org/10.1016/j.celrep.2023.112601.
[40] K.A. White, B.K. Grillo-Hill, D.L. Barber, Cancer cell behaviors mediated by dysregulated pH dynamics at a glance, J. Cell Sci. 130 (2017) 663–669, https://doi.org/10.1242/jcs.195297.
[41] G. Hao, Z.P. Xu, L. Li, Manipulating extracellular tumour pH: an effective target for cancer therapy, RSC Adv. 8 (2018) 22182–22192, https://doi.org/10.1039/c8ra02095g.
[42] P. Swietach, R.D. Vaughan-Jones, A.L. Harris, A. Hulikova, The chemistry, physiology and pathology of pH in cancer, Philos. Trans. R. Soc. B Biol. Sci. 369 (2014), https://doi.org/10.1098/rstb.2013.0099.
[43] D. Corinti, C. Coletti, N. Re, S. Piccirillo, M. Giampà, M.E. Crestoni, S. Fornarini, Hydrolysis of cis- and transplatin: structure and reactivity of the aqua complexes in a solvent free environment, RSC Adv. 7 (2017) 15877–15884, https://doi.org/10.1039/C7RA01182B.
[44] N.D. Eljack, H.Y.M. Ma, J. Drucker, C. Shen, T.W. Hambley, E.J. New, T. Friedrich, R.J. Clarke, Mechanisms of cell uptake and toxicity of the anticancer drug cisplatin, Metallomics 6 (2014) 2126–2133, https://doi.org/10.1039/c4mt00238e.
[45] H.E. Gottlieb, V. Kotlyar, A. Nudelman, NMR Chemical Shifts of Common Laboratory Solvents as Trace Impurities In the Course of the Routine Use of NMR as an Aid for Organic Chemistry, a Day-to-Day Problem is the Identifica- tion of Signals Deriving from Common Contaminants Literature, But the, 3263, 1997, pp. 7512–7515.
[46] N.R. Babij, E.O. McCusker, G.T. Whiteker, B. Canturk, N. Choy, L.C. Creemer, C.V. D. Amicis, N.M. Hewlett, P.L. Johnson, J.A. Knobelsdorf, F. Li, B.A. Lorsbach, B. M. Nugent, S.J. Ryan, M.R. Smith, Q. Yang, NMR chemical shifts of trace impurities: industrially preferred solvents used in process and green chemistry, Org. Process. Res. Dev. 20 (2016) 661–667, https://doi.org/10.1021/acs.oprd.5b00417.
[47] M. J. Frisch, G. W. Trucks, H. B. Schlegel, G. E. Scuseria, M. A. Robb, J. R. Cheeseman, G. Scalmani, V. Barone, G. A. Petersson, H. Nakatsuji, X. Li, M. Caricato, A. Marenich, J. Bloino, B. G. Janesko, R. Gomperts, B. Mennucci, H. P. Hratchian, J. V. Ort, D.J. Fox, Gaussian09 Revision D.01, Gaussian09 Revis. D.01 (n.d.).
[48] M. Frisch, G. Trucks, H. Schlegel, G. Scuseria, M. Robb, J. Cheeseman, G. Scalmani, V. Barone, G. Petersson, H. Nakatsuji, X. Li, M. Transport, A. Marenich, J. Bloino, B. Janesko, R. Gomperts, B. Mennucci, H. Hratchian, D. Gaussian, Gaussian 16, Révision B.01 6, Inc Wallingford CT, 2016.
[49] I. Płowaś, J. Świergiel, J. Jadzyn, Relative static permittivity of dimethyl sulfoxide + water mixtures, J. Chem. Eng. Data 58 (2013) 1741–1746, https://doi.org/10.1021/je400149j.
[50] S.A. Markarian, A.M. Terzyan, Surface tension and refractive index of dialkylsulfoxide + water mixtures at several temperatures, J. Chem. Eng. Data 52 (2007) 1704–1709, https://doi.org/10.1021/je7001013.
[51] M.W. Lodewyk, M.R. Siebert, D.J. Tantillo, Computational prediction of 1H and 13C chemical shifts: a useful tool for natural product, mechanistic, and synthetic organic chemistry, Chem. Rev. 112 (2012) 1839–1862, https://doi.org/10.1021/cr200106v.
[52] G.K. Pierens, 1H and 13C NMR scaling factors for the calculation of chemical shifts in commonly used solvents using density functional theory, J. Comput. Chem. 35 (2014) 1388–1394, https://doi.org/10.1002/jcc.23638.
[53] http://cheshireNMR.info, (n.d.).
[54] P.J. Hay, W.R. Wadt, Ab initio effective core potentials for molecular calculations. Potentials for K to au including the outermost core orbitale, J. Chem. Phys. 82 (1985) 299–310, https://doi.org/10.1063/1.448975.
[55] A.K. Rappé, C.J. Casewit, K.S. Colwell, W.A. Goddard, W.M. Skiff, UFF, a full periodic table force field for molecular mechanics and molecular dynamics simulations, J. Am. Chem. Soc. 114 (1992) 10024–10035, https://doi.org/10.1021/ja00051a040.
[56] M. Samiei, S. Shahi, N. Aslaminabadi, H. Valizadeh, Z. Aghazadeh, S.M.V. Pakdel, A new simulated plasma for assessing the solubility of mineral trioxide aggregate, Iran, Aust. Endod. J. 10 (2015) 30–34.